Virasoro generators in the Fibonacci model tensor network: Tackling finite-size effects

Xiangdong Zeng,[1,2] Ruoshui Wang,[3,4] Ce Shen,[1,2] and Ling-Yan Hung[1,2,5,6,*]

[1]*State Key Laboratory of Surface Physics, Fudan University, Shanghai 200433, China*
[2]*Department of Physics and Center for Field Theory and Particle Physics, Fudan University, Shanghai 200433, China*
[3]*Department of Physics, Cornell University, Ithaca, New York 14853, USA*
[4]*Institute for Advanced Study, Tsinghua University, Beijing 100084, China*
[5]*Institute for Nanoelectronic Devices and Quantum Computing, Fudan University, Shanghai 200433, China*
[6]*Yau Mathematical Sciences Center, Tsinghua University, Beijing 100084, China*

(Received 12 December 2022; revised 23 March 2023; accepted 18 May 2023; published 30 June 2023)

In this paper, we extend the method implementing Virasoro operators in a tensor network we proposed in Wang *et al.* [Phys. Rev. B **106**, 115116 (2022)] and test it on the Fibonacci model, which is known to suffer from far more finite-size effects. To pick up the "seed" state that would flow to the stress tensor in the thermodynamic limit, we make use of the topological idempotent that projects the transfer matrix to the trivial sector. Combined with an optimization method, the seed state can be identified. We demonstrate that the descendant states in the Fibonacci model can be correctly generated with this approximate stress tensor, giving further evidence that the method applies more generally.

DOI: 10.1103/PhysRevB.107.245146

I. INTRODUCTION

There is a lot of progress in the last few years in recovering data of a continuous field theory from lattice models in a controlled numerical setting making use of tensor networks [1–11]. Particularly, in the case of two-dimensional (2D) conformal field theories (CFTs), there is by now a lot of work on extracting the CFT spectra from the tensor networks. More recently, there are works developing methodologies to understand how conformal and other (continuous) symmetries are realized on the tensor networks [3,7,8,12,13].

These methods mainly focus on constructing discrete operators that act on a one-dimensional lattice Hilbert space. However, they are not immediately applicable when we work on tensor networks that directly reconstruct the 2D partition functions. Frequently, we combine with tensor renormalization algorithms so that individual tensors building up the tensor network representation of the partition function are known only numerically, making it technically difficult to recover the Hamiltonian picture by taking the time evolution $\Delta t \to 0$ limit. In [14], we proposed a method to implement the Virasoro symmetries from the intuitive picture that the insertion of Virasoro operators is equivalent to the insertion of the stress tensor with appropriate weight around a closed loop. We implement stress tensor insertion by solving for the eigenstates of the transfer matrix tiling a cylinder, which is related to the dilatation operator through a conformal map. By the state-operator correspondence, these eigenstates represent a small disk with the stress tensor inserted at its center. These small disks are then inserted around a large disk to extract Virasoro descendants of the state corresponding to the large disk. We demonstrated this method in the case of the Ising model and found that this naive method appears to work quite well.

The Ising model is known to be very special and suffers from less severe finite-size effects. In this paper, we would like to inspect our proposal in other models where finite-size effects are more severe. Particularly, we will consider the $\mathbb{Z}_3$ parafermion CFT, which can be obtained by giving appropriate boundary conditions to the Fibonacci Levin-Wen topological order. Here, the spectrum of a cylinder of intermediate sizes would still look quite far from the actual CFT spectrum. This, however, does not mean that we cannot extract anything useful out of it. As the cylinder gets bigger, the spectrum would approach that of the CFT, and there is a sense of continuity in the process of solving for eigenstates for cylinders of larger and larger sizes. It is well known that one can record the respective eigenvalues as cylinder size grows and this allows one to extract the asymptotic eigenvalues numerically with only cylinders of finite size. See, for example, [1,6,15,16].

In this paper, we will explain how we can pick up the eigenstate of a cylinder that would flow towards the stress tensor. A technical complication arises here, since the stress tensor is a fairly excited state in the spectrum, unlike in the case of the Ising model (we briefly reviewed the calculation of the Ising CFT spectrum in the Supplemental Material [17]), making it more cumbersome to identify the eigenstate that would eventually flow to the actual stress tensor. To help identify the stress tensor, we make use of the projector constructed in [1,6,15,16,18]. It can be constructed using the tube algebra method [19,20], and can project transfer matrix into sectors with definite topological charges. In the case of the stress tensor, it belongs to the trivial sector. Since the topological charges are explicit down to the smallest lattice scale in the

*lyhung@fudan.edu.cn

lattice realization based on the string-net model, the eigenstate that could possibly flow to the stress tensor in the thermodynamic limit should still be found in the topologically trivial sector. The projector thus helps to remove a large number of states from other sectors. With the help of the projector, we identify the "seed" stress tensor which is used to construct the Virasoro operator that can be applied to a disk. We demonstrate that it generates descendants in the disk to an acceptable accuracy.

The paper is organized as follows. We will first review the tensor network construction of these lattice partition functions based on the Levin-Wen models. Then we will provide details of the transfer matrix of the Fibonacci model and construct the appropriate projector. Finally, we will demonstrate the construction of the Virasoro operator.

II. TENSOR NETWORK CONSTRUCTION OF LATTICE TRANSFER MATRICES

A. Strange correlators

It is observed that families of partition function Z of some lattice models can be expressed as a *strange correlator* [6,18], which is obtained by taking the overlap between the ground state wave function of a topological order $|\Psi\rangle$ with some direct product state $\langle\Omega|$. For concreteness, these topological orders are chosen to be those represented by the Levin-Wen string-net model, i.e.,

$$Z = \langle\Omega|\Psi_{\mathrm{SN}}\rangle. \tag{1}$$

When $\langle\Omega|$ is tuned appropriately, the partition function would describe a 2D CFT in the thermodynamic limit.

Practically, the ground state wave function of a given string-net model defined by a fusion category $\mathcal{C}$ can be constructed as a projected entangled pair state (PEPS) tensor network [6,15,18,21,22]. We will make heavy use of the notations introduced in [6,15]. The general tensor unit of a trivalent PEPS graph is given by

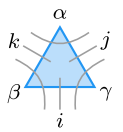

$$= D^{-2(1/n_\alpha+1/n_\beta+1/n_\gamma)}\left(d_\alpha^{1/n_\alpha} d_\beta^{1/n_\beta} d_\gamma^{1/n_\gamma}\right) \cdot (d_i d_j d_k)^{-\frac{1}{4}} (d_\alpha d_\beta d_\gamma)^{-\frac{1}{2}}$$

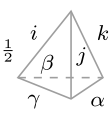

, (2)

where d_i is the *quantum dimension* of simple object i belonging to $\mathcal{C}$, D is the *total quantum dimension* of $\mathcal{C}$, and n_α is the number of equal-length arcs in the closed loop containing α. Each tetrahedron is assigned a value related to the F symbols of the string-net model as follows:

$$= \sqrt{d_i d_j d_k d_l}\left[F_l^{ijk}\right]_{mn}. \tag{3}$$

The ground state wave function $|\Psi_{\mathrm{SN}}\rangle$, or the PEPS tensor network, is then constructed by assembling these building blocks, with the edge degrees of freedom playing the role of physical legs of the wave function, and the corner degrees of freedom summed over:

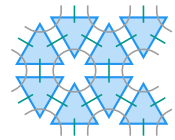

where | = physical leg, | = virtual leg. (4)

By fixing the physical legs of the wave function to some particular linear combinations (i.e., taking inner product with $\langle\Omega|$), the strange correlator can be obtained.

Fibonacci string-net is defined on the hexagonal lattice. There are two objects, $\mathbf{1}$ and τ with quantum dimension $d_{\mathbf{1}} = 1$, $d_\tau = \varphi$, where $\varphi = (1+\sqrt{5})/2$ is the golden ratio. The only nontrivial fusion rule and F symbol are

$$\tau \times \tau = \mathbf{1} + \tau, \quad F_\tau^{\tau\tau\tau} = \varphi^{-1}\begin{pmatrix} 1 & \sqrt{\varphi} \\ \sqrt{\varphi} & -1 \end{pmatrix}. \tag{5}$$

The only nonvanishing tetrahedron and the corresponding triangle tensor are

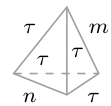

$$= \sqrt{d_\tau d_\tau d_\tau d_\tau}\left[F_\tau^{\tau\tau\tau}\right]_{mn} = \varphi^2\left[F_\tau^{\tau\tau\tau}\right]_{mn},$$

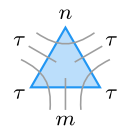

$$= (d_\tau d_\tau d_m)^{-\frac{1}{4}}(d_\tau d_\tau d_n)^{-\frac{1}{3}}$$

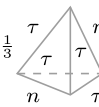

$$= \varphi^{\frac{5}{6}} d_m^{-\frac{1}{4}} d_n^{-\frac{1}{3}}\left[F_\tau^{\tau\tau\tau}\right]_{mn}, \quad m,n \in \{\mathbf{1},\tau\}. \tag{6}$$

In our strange correlator construction, all the physical legs are fixed to τ (i.e., $m = \tau$). So there will be only two kinds of triangle tensor units:

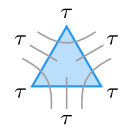

$$= \varphi^{\frac{1}{4}}\left[F_\tau^{\tau\tau\tau}\right]_{\tau\tau} = -\varphi^{-\frac{3}{4}},$$

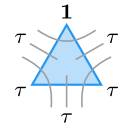

$$= \varphi^{\frac{7}{12}}\left[F_\tau^{\tau\tau\tau}\right]_{\tau\mathbf{1}} = \varphi^{\frac{1}{12}}. \tag{7}$$

B. Cylinder transfer matrices

The tensor units of Fibonacci string-net (7) are triangles. To calculate the corresponding spectrum conveniently, we first build a four-leg tensor (a square) with a pair of triangles:

$$A_{ijkl} =$$

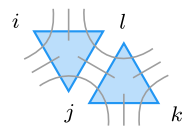

$$=$$

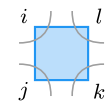

. (8)

Using such a tensor unit, we would like to construct the transfer matrix M, which is the discrete version of the path integral of the CFT on a cylinder. Consider putting the basic

TABLE I. Fibonacci spectrum from transfer matrices of different sizes. Vacuum state and its descendants (marked with bold blue) are obtained by diagonalizing the transfer matrix with idempotents (see Sec. III C). The cylinder sizes are from 12 to 27 and are extrapolated to infinity, with data listed in the "∞" column.

SpinSize	9	12	15	18	21	24	27	∞	Rescaled	Exact
0	0.0	0.0	0.0	0.0	0.0	0.0	0.0	0.0	0.0	0
0[a]	0.112899	0.113952	0.114474	0.114769	0.114950	0.115070	0.115152	0.11610 (7)	0.1513 (32)	$\frac{2}{15}$
0	0.722756	0.709100	0.703083	0.699890	0.697989	0.696765	0.695931	0.6856 (9)	0.894 (19)	$\frac{4}{5}$
±1	0.785553	0.817591	0.841528	0.859630	0.873686	0.884880	0.893989	0.9557 (27)	1.246 (27)	$1+\frac{2}{15}$
±1	1.594955	1.346025	1.242196	1.184631	1.147942	1.122492	1.103796	0.914 (11)	1.191 (29)	$1+\frac{2}{15}$
0[a]	1.290074	1.222673	1.196184	1.182805	1.175050	1.170137	1.166820	1.123 (4)	1.464 (32)	$\frac{4}{3}$
±1	1.147427	1.222649	1.274342	1.312081	1.340887	1.363620	1.382029	1.510 (4)	1.97 (4)	$1+\frac{4}{5}$
±1	3.221770	2.490495	2.169235	2.016147	1.925379	1.865017	1.821876	1.31 (5)	1.70 (8)	$1+\frac{4}{5}$
±2	2.727358[b]	2.139950	1.967143	1.887302	1.842910	1.815429	1.797149	1.535 (33)	2.00 (6)	2
±2	1.032723[b]	1.178227	1.276463	1.348394	1.403716	1.447739	1.483672	1.730 (9)	2.25 (5)	$2+\frac{2}{15}$
±2	–[b]	1.430687	1.484488	1.527193	1.561317	1.589035	1.611935	1.759 (9)	2.29 (5)	$2+\frac{2}{15}$

[a]There is twofold degeneracy in these levels.
[b]For the $n = 9$ cylinder, the transfer matrix is not large enough, so some high-level descendants may not show up; at the same time, spin ±2 will degenerate to ±1.

tensor units together to form a ring:

$$\tilde{M}_{i_1 i_2 \cdots i_n, j_1 j_2 \cdots j_n} = \sum_{\substack{i_1,i_2,\ldots,i_n \\ j_1,j_2,\ldots,j_n}} \prod_{\alpha=1}^{n} A_{i_\alpha j_\alpha j_{\alpha+1} i_{\alpha+1}}$$

$$= \quad (9)$$

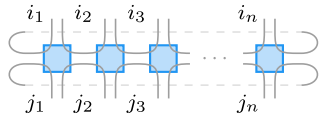

Different from the square-lattice case (e.g., typically in the 2D Ising model), the indices of A_{ijkl} are placed at corners, so they should be connected carefully in the particular order and orientation during contractions. Furthermore, the above cylinder $\tilde{M}$ is still not sufficient for a correct transfer matrix that is equal only to the exponentiation of the Hermitian. If we stack these cylinders row by row, the result will be a slanted cylinder and an additional phase will appear in the final spectrum. By putting two copies of cylinders with opposite orientations together, i.e., taking

$$M = \tilde{M}\tilde{M}^{\dagger}, \quad (10)$$

this phase can be removed.

As discussed in [2,14], we can obtain the CFT spectrum by diagonalizing TM, where T is the translation operator. In the tensor network representation, T is simply given by shifting the lattice by one site:

$$T_{i_1 i_2 \cdots i_n, j_1 j_2 \cdots j_n} =$$

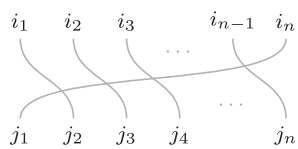

(11)

III. CFT SPECTRUM OF FIBONACCI STRING NET

A. Calculation

In the thermodynamic limit, the Fibonacci string net (critical hard-hexagon model with $c = 4/5$ [6]) approaches the $\mathbb{Z}_3$ parafermion CFT, but not all topological defects of the continuum CFT ($\mathbb{Z}_3 \otimes$ Fib) have matrix product operator (MPO) representations in this specific lattice model [6]. Therefore, to get the "empty" torus partition function without nontrivial topological defects, we have to look at a transfer matrix with $n = 3k$ sites. Correspondingly, we should use a three-site translation operator (or T^3) as well.

The memory consumption for the above construction grows exponentially with cylinder size n. To practically perform the calculation, we need to store the transfer matrix in the form of linear operators [23]. The basic idea is that retaining the whole tremendous matrix in the memory is unnecessary; instead, what we need is the matrix-vector multiplication of this transfer matrix as an "operator." Due to the nature of tensor network representation, it is not difficult to construct such a multiplication function. The details of the implementation are given in the Supplemental Material [17].

B. Spectrum of the transfer matrix

The spectrum data are listed in Table I. The Fibonacci model suffers from significant finite-size effects and hence only cylinders with size $n \gtrsim 20$ can give a relatively accurate result. For small cylinders, some excitation states may not even show up among the low-lying states. In principle, we can separate different states based on their scaling dimensions and conformal spins. But due to the finite-size effects, not only are the eigenvalues far from their limiting CFT values, there are also ubiquitous issues with level crossing—some supposedly highly excited states in the thermodynamic limit pick up small eigenvalues when the cylinder is small, which makes it difficult to distinguish them. Here, we assume that the scaling dimensions Δ will approach the thermodynamic limiting values as $\Delta = A + B/n$ [24] and we optimize the fitting results by selecting eigenstates of the small cylinder that actually flow to the desired CFT conformal states (i.e., choose the point nearest to the fitting curve; see the Supplemental Material [17] for details). The "∞" column in Table I

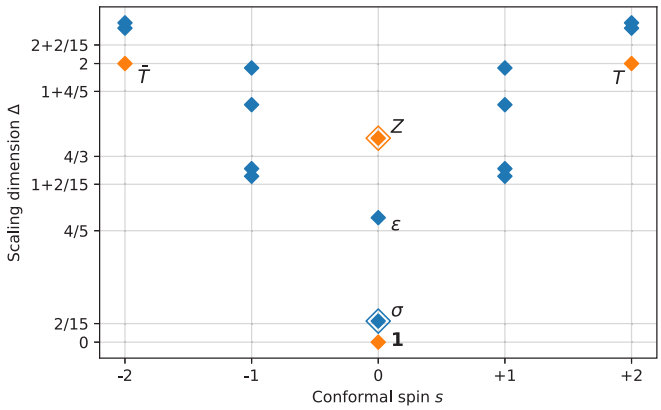

FIG. 1. Fibonacci spectrum corresponding to the cylinder transfer matrix of size $n \to \infty$. "◈" indicates that there is a twofold degeneracy. The values have been rescaled so that $\Delta_{\mathbf{1}} = 0$ and $\Delta_T = 2$. Primary states are labeled with their corresponding operators, with conformal dimensions $h_{\mathbf{1}} = 0$, $h_\sigma = 1/15$, $h_\epsilon = 2/5$, $h_Z = 2/3$, $h_X = 7/5$, and $h_Y = 3$, respectively (states corresponding to X and Y are higher and they are not considered in our calculation). The CFT partition function is then $Z = |\chi_{\mathbf{1}} + \chi_Y|^2 + |\chi_\epsilon + \chi_X|^2 + 2|\chi_\sigma|^2 + 2|\chi_Z|^2$ [6]. The states that lie within the subspace corresponding to the trivial sector $|\chi_{\mathbf{1}} + \chi_Y|^2$ are drawn in orange.

is obtained by extrapolating cylinder size $n \to \infty$ (equal to A in the above formula). To estimate the scaling dimension more accurately, we can fix the identity state $|\phi_{\mathbf{1}}\rangle$ and state $|\phi_T\rangle$ corresponding to the stress tensor such that $\Delta_{\mathbf{1}} = 0$ and $\Delta_T = 2$:

$$\Delta_\alpha = \frac{2}{\log \lambda_T - \log \lambda_I}(\log \lambda_\alpha - \log \lambda_I), \tag{12}$$

where λ_α are the corresponding eigenvalues. The results are listed in the "Rescaled" column and plotted in Fig. 1. When there are many states mingled together, however, the optimization procedure is troublesome and may not be guaranteed to find the correct state. To simplify the task, we make use of the projector mentioned in the Introduction. It was constructed in [6,15,18,22,25], which would project the transfer matrix to a subspace with definite topological charge. For the stress tensor, it belongs to the trivial sector, whose corresponding projector can be readily employed. In the next section, we will describe the construction of the needed idempotent in detail.

C. Topological projectors

In the PEPS representation of the string-net models, each type of anyons of the topological model has a corresponding string operator. Their construction is related to the so-called Ocneanu's tube algebra. Each type of anyon in the topological model corresponds to a topological sector of the CF, i.e., the families of primaries in the CFT can be organized into different topological sectors, each corresponding to an anyon of the topological model. Each string operator constructed in the topological model behaves as a projector that can project the CFT transfer matrix on a cylinder down to a subspace containing states in this corresponding topological sector. Since we are particularly interested in obtaining the stress tensor, which belongs to the trivial sector in the topological model, we need the corresponding string operator. These operators take the form of MPOs that have been systematically constructed in [6,15,18,22,25], and they are often referred to as the *idempotents*. We will review the needed ingredients below.

The tensor unit of such MPO is given by

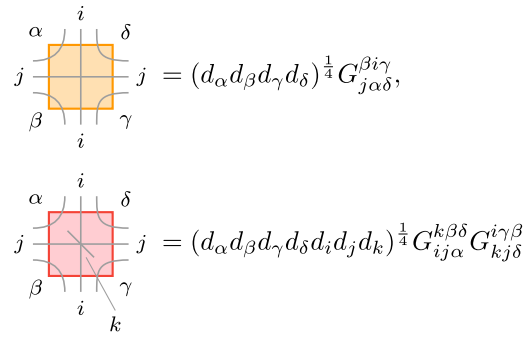

(13)

where G is a normalized and symmetric version of the tetrahedron:

$$G^{abc}_{ijk} = \frac{1}{\sqrt{d_j d_c}} \left[F^{aik}_b\right]_{jc} = \frac{1}{\sqrt{d_a d_b d_c d_i d_j d_k}}$$

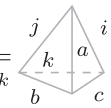

. (14)

For the cylinder transfer matrix of size n, the tube algebra basis is then given by a chain of $n-1$ orange tensors with a red one connected at the end (virtual legs to be contracted are omitted here):

$\mathcal{T}^c_{ab} =$

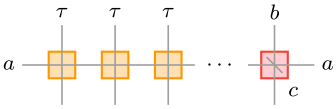

. (15)

In general, the idempotents are linear combinations of these basis tensors, and the calculation of their coefficients can be found in Appendix C of [22]. Here, our aim is to identify the stress tensor that is the descendant of the vacuum state, so we need to use the idempotent projecting to the trivial sector. This is given by

$$\mathcal{P}_{\mathbf{1}} = \frac{1}{\sqrt{5}}\left(\frac{1}{\phi}\mathcal{T}^{\mathbf{1}}_{\mathbf{11}} + \sqrt{\phi}\mathcal{T}^{\tau}_{\tau\mathbf{1}}\right). \tag{16}$$

Then it can be stacked to the transfer matrix (9) with translation operator (11). In Fig. 1, the states that lie within the subspace preserved by $\mathcal{P}_{\mathbf{1}}$ are drawn in orange. The stress tensor T lies within this trivial sector, with many other intervening states with similar conformal dimensions removed. This allows us to recover the correct seed state that flows to the stress tensor.

IV. VIRASORO OPERATOR

Our method for constructing the Virasoro operator in lattice models is inspired by the success of "discrete holomorphicity," a substantial subject reviewed, for example, in [26]. The basic idea is that a lattice version of contour integral can be approximated by discretely inserting operators along

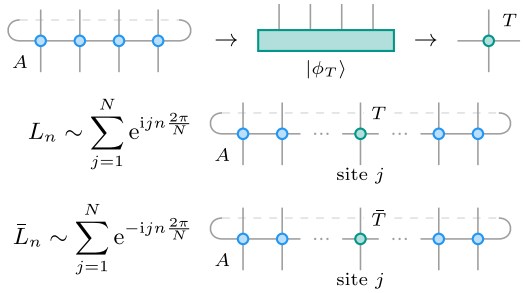

FIG. 2. Tensor network implementation of Eq. (17). Eigenstate $|\phi_T\rangle$ corresponding to the stress tensor is solved from the cylinder transfer matrix [the one shown in the top left is only schematic; for details of it one should refer to Eqs. (9), (10), and (11)]. It has been reshaped to a four-leg tensor and then inserted into a new cylinder to construct the Virasoro operators.

the intended path. In [14] we made the following proposal to implement Virasoro operators in a tensor network. We take the following definitions of the Virasoro operators in the continuous theory

$$L_n \sim \sum_{j=1}^{N} e^{ijn(2\pi/N)} T(j), \quad \bar{L}_n \sim \sum_{j=1}^{N} e^{-ijn(2\pi/N)} \bar{T}(j) \tag{17}$$

and take them seriously in a tensor network, by replacing the operator insertion at a point by the state we solved from the transfer matrix above at the vertex labeled j. Here, $T(j)$ and $\bar{T}(j)$ are eigenstates of the cylinder transfer matrix of finite size we found in previous sections. With the help of idempotents and optimization, they are deemed to flow towards the actual CFT states corresponding to the stress tensor in the thermodynamic limit. The insertion procedure is depicted in Fig. 2.

Since the cylinder's size has to be $n = 3k$ for the Fibonacci case, we cannot directly insert the stress tensor T and $\bar{T}$ into the new cylinder as it requires a four-leg unit. Instead, we need to first reshape it into a triangle and then pad with "empty" triangle tensors Eq. (7) to obtain a square one, analogous to the tensor constructed in Eq. (8):

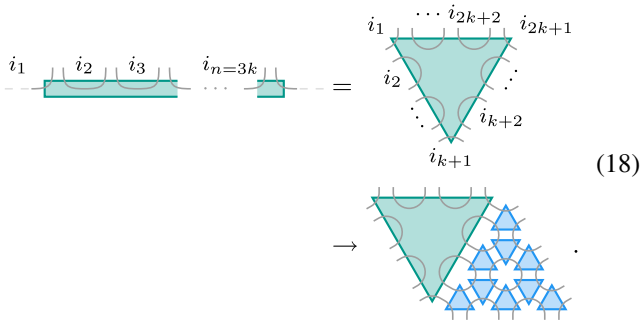

(18)

Note that the contraction only involves the corner degrees of freedom. For the other sites of the new cylinder, we can build them in the same way. To make the contraction more efficient, however, we can block $k \times k$ square tensors in Eq. (8) as the unit equivalently.

In our calculation, we take cylinder sizes $n = 12$, 15, and 18 to find the eigenstates corresponding to the stress tensor. They are reshaped and padded into four-leg tensor units with

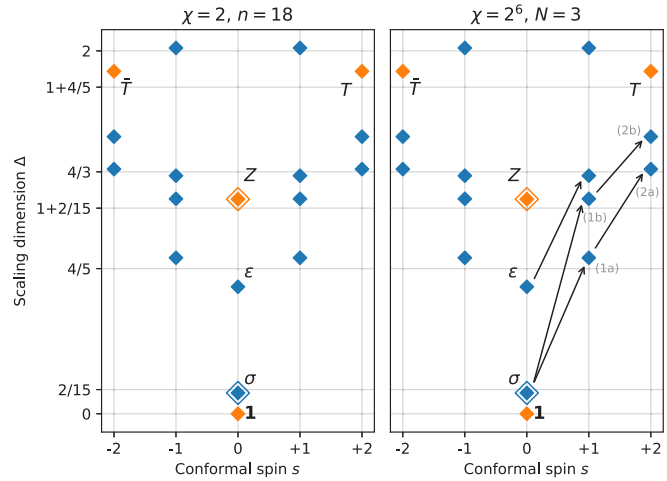

FIG. 3. We use the cylinder of size $n = 18$ to solve for the stress tensor (left). T and $\bar{T}$ are used to build the Virasoro operators L_n and $\bar{L}_n$ in a new cylinder of size $N = 3$ and bond dimension $\chi = 2^{n/3}$. The actions of L_{-1} are illustrated by the arrows as an example (right). The states labeled (1a)/(1b) and (2a)/(2b) should be degenerate at the CFT limit but are split here due to the finite-size effect (cf. Fig. 1). Note that to be consistent with the data in the Supplemental Material [17], the scaling dimensions shown here are *not* rescaled.

bond dimension $\chi = 2^{n/3}$. Then we use these tensor units as well as the blocking sites to form a new cylinder for obtaining the Virasoro operator. In principle, the size of the new cylinder N, which is composed of these reshaped tensors with large bond dimension, can be chosen arbitrarily. But due to the limit of memory resource, we have to take an $N = 3$ cylinder (equivalent to the n-site cylinder with bond dimension $\chi = 2$) for the calculation of the stress tensor in reality. We check their validity by applying these operators to low-energy eigenstates (same from size N cylinder) and see if they will be correctly raised or lowered into certain levels. We show the actions of L_{-1} in Fig. 3, and more numerical results on the action of L_{+1}, L_{-2}, and L_{+2} are included in the Supplemental Material [17].

V. CONCLUSIONS

In this paper, we inspect our proposal of implementing Virasoro symmetry in a tensor network in a more elaborate lattice model than the Ising model. Particularly, we worked with the Fibonacci model, which is known to suffer from more severe finite-size effects. The method that we have proposed continues to work reasonably well, although in this case, to extract the stress tensor from a relatively small transfer matrix tiling a small cylinder, we need to make use of the method of the idempotent, to project out states with different topological charges. Paired with the optimization procedure which fits the eigenvalues in a power law as it approaches the thermodynamic limit, we can isolate the appropriate "seed" state that would flow to the stress tensor. We show that using a seed state to construct a Virasoro operator still produces reasonably accurate descendants in a cylinder that is marred by finite-size effects. This complements our earlier

work, giving further evidence with an improved algorithm for reconstructing Virasoro symmetry in a more general tensor network.

ACKNOWLEDGMENTS

L.-Y.H. acknowledges the support of NSFC (Grants No. 11922502 and No. 11875111) and the Shanghai Municipal Science and Technology Major Project (Shanghai Grant No. 2019SHZDZX01), and Perimeter Institute for hospitality as a part of the Emmy Noether Fellowship Programme. We are particularly grateful to Frank Verstraete and Robijn Vanhove for multiple correspondences, explaining in detail the methodologies they employed in their series of papers. We also thank Lin Chen, Jiaqi Lou, Bingxin Lao, and Xinyang Yu for useful discussions and comments.

[1] G. Evenbly and G. Vidal, Local Scale Transformations on the Lattice with Tensor Network Renormalization, Phys. Rev. Lett. **116**, 040401 (2016).
[2] M. Hauru, G. Evenbly, W. W. Ho, D. Gaiotto, and G. Vidal, Topological conformal defects with tensor networks, Phys. Rev. B **94**, 115125 (2016).
[3] A. Milsted and G. Vidal, Extraction of conformal data in critical quantum spin chains using the Koo-Saleur formula, Phys. Rev. B **96**, 245105 (2017).
[4] S. Yang, Z.-C. Gu, and X.-G. Wen, Loop Optimization for Tensor Network Renormalization, Phys. Rev. Lett. **118**, 110504 (2017).
[5] M. Bal, M. Mariën, J. Haegeman, and F. Verstraete, Renormalization Group Flows of Hamiltonians Using Tensor Networks, Phys. Rev. Lett. **118**, 250602 (2017).
[6] R. Vanhove, M. Bal, D. J. Williamson, N. Bultinck, J. Haegeman, and F. Verstraete, Mapping Topological to Conformal Field Theories through Strange Correlators, Phys. Rev. Lett. **121**, 177203 (2018).
[7] Y. Zou, A. Milsted, and G. Vidal, Conformal Data and Renormalization Group Flow in Critical Quantum Spin Chains Using Periodic Uniform Matrix Product States, Phys. Rev. Lett. **121**, 230402 (2018).
[8] Y. Zou, A. Milsted, and G. Vidal, Conformal Fields and Operator Product Expansion in Critical Quantum Spin Chains, Phys. Rev. Lett. **124**, 040604 (2020).
[9] Y. Zou and G. Vidal, Emergence of conformal symmetry in quantum spin chains: Antiperiodic boundary conditions and supersymmetry, Phys. Rev. B **101**, 045132 (2020).
[10] T.-C. Huang, Y.-H. Lin, K. Ohmori, Y. Tachikawa, and M. Tezuka, Numerical Evidence for a Haagerup Conformal Field Theory, Phys. Rev. Lett. **128**, 231603 (2022).
[11] R. Vanhove, L. Lootens, M. Van Damme, R. Wolf, T. J. Osborne, J. Haegeman, and F. Verstraete, Critical Lattice Model for a Haagerup Conformal Field Theory, Phys. Rev. Lett. **128**, 231602 (2022).
[12] W. Koo and H. Saleur, Representations of the Virasoro algebra from lattice models, Nucl. Phys. B **426**, 459 (1994).
[13] R. Wang, Y. Zou, and G. Vidal, Emergence of Kac-Moody symmetry in critical quantum spin chains, Phys. Rev. B **106**, 115111 (2022).
[14] R. Wang, X. Zeng, C. Shen, and L.-Y. Hung, Virasoro and Kac-Moody algebra in generic tensor network representations of two-dimensional critical lattice partition functions, Phys. Rev. B **106**, 115116 (2022).
[15] D. J. Williamson, N. Bultinck, and F. Verstraete, Symmetry-enriched topological order in tensor networks: Defects, gauging and anyon condensation, arXiv:1711.07982.
[16] L. Lootens, R. Vanhove, J. Haegeman, and F. Verstraete, Galois Conjugated Tensor Fusion Categories and Nonunitary Conformal Field Theory, Phys. Rev. Lett. **124**, 120601 (2020).
[17] See Supplemental Material at http://link.aps.org/supplemental/10.1103/PhysRevB.107.245146 for more technical details and numerical results.
[18] D. Aasen, P. Fendley, and R. S. Mong, Topological defects on the lattice: Dualities and degeneracies, arXiv:2008.08598.
[19] D. E. Evans and Y. Kawahigashi, On Ocneanu's theory of asymptotic inclusions for subfactors, topological quantum field theories and quantum doubles, Int. J. Math. **06**, 205 (1995).
[20] D. E. Evans and Y. Kawahigashi, *Quantum Symmetries on Operator Algebras* (Clarendon, Oxford, 1998), Vol. 147.
[21] O. Buerschaper, M. Aguado, and G. Vidal, Explicit tensor network representation for the ground states of string-net models, Phys. Rev. B **79**, 085119 (2009).
[22] N. Bultinck, M. Mariën, D. Williamson, M. Şahinoğlu, J. Haegeman, and F. Verstraete, Anyons and matrix product operator algebras, Ann. Phys. **378**, 183 (2017).
[23] P. Virtanen, R. Gommers, T. E. Oliphant, M. Haberland, T. Reddy, D. Cournapeau, E. Burovski, P. Peterson, W. Weckesser, J. Bright, S. J. van der Walt, M. Brett, J. Wilson, K. J. Millman, N. Mayorov, A. R. J. Nelson, E. Jones, R. Kern, E. Larson, C. J. Carey *et al.*, SciPy 1.0: Fundamental algorithms for scientific computing in python, Nat. Methods **17**, 261 (2020).
[24] M. Schuler, S. Whitsitt, L.-P. Henry, S. Sachdev, and A. M. Läuchli, Universal Signatures of Quantum Critical Points from Finite-Size Torus Spectra: A Window into the Operator Content of Higher-Dimensional Conformal Field Theories, Phys. Rev. Lett. **117**, 210401 (2016).
[25] L. Lootens, R. Vanhove, and F. Verstraete, Cardy states, defect lines and chiral operators of coset CFTs on the lattice, arXiv:1907.02520.
[26] J. Cardy, Discrete holomorphicity at two-dimensional critical points, J. Stat. Phys. **137**, 814 (2009).